

# Theoretical Study of Electronic Structure, Formation Mechanism and Intramolecular Sulfoxide Imidation Reactivity of Iron Phthalocyanine Nitrene Complex<sup>①</sup>

YUAN Bin-Bin<sup>a, b</sup> SONG Jin-Shuai<sup>a②</sup> YAN Xue-Yuan<sup>a, b</sup>  
XIAO Han<sup>a, b</sup> LI Chun-Sen<sup>a, b, c②</sup>

<sup>a</sup> (State Key Laboratory of Structural Chemistry, Fujian Institute of Research on the Structure of Matter, Chinese Academy of Sciences, Fuzhou 350002, China)

<sup>b</sup> (University of Chinese Academy of Sciences, Beijing 100049, China)

<sup>c</sup> (Fujian Provincial Key Laboratory of Theoretical and Computational Chemistry, Xiamen 361005, China)

**ABSTRACT** Density functional theory (DFT) calculations are performed to investigate recent experimentally studied ring-closing sulfoxide imidation catalyzed by Fe(II)-phthalocyanine (Fe<sup>II</sup>Pc). Our results reveal that the ground state of iron phthalocyanine nitrene intermediate (PcFeNR, R = (CH<sub>2</sub>)<sub>3</sub>(SO)Ph), which is believed to mediate the intramolecular imidation, is triplet state featuring a diradical structure. The formation of PcFeNR is the result of a denitration process with a calculated high-barrier of 23.4 kcal/mol which is in good agreement with the experimentally observed high reaction temperature of 100 °C. The generated PcFeNR undergoes a low-barrier intramolecular nucleophilic attack by proximal nitrogen atom on the sulfur accomplishing the cyclization of sulfoxide. This study provides theoretical insights into the mechanism-based design of useful catalysts for nitrene transfer reactions.

**Keywords:** nitrene transfer, sulfoxide cyclization, iron phthalocyanine, DFT, reaction mechanism;

**DOI:** 10.14102/j.cnki.0254-5861.2011-2956

## 1 INTRODUCTION

Transition metal-nitrene complexes have been proved to be appealing reactive intermediates in the synthesis of versatile N-substituted pharmaceutical products<sup>[1]</sup>, agrochemicals, and synthetic precursors, especially after the success of characterizing such unstable species<sup>[2, 3]</sup>. Iminoiodanes (*i.e.* PhI = NTs)<sup>[4-8]</sup>, haloamine-T compounds<sup>[9, 10]</sup> and carbamates<sup>[11]</sup> are widely accepted nitrene sources for many years. Recently, organic azides are becoming the new promising green nitrene alternatives with harmless nitrogen as the only byproduct<sup>[12, 13]</sup>. For a long time, the noble metal (*i.e.* rhodium<sup>[14, 15]</sup>, ruthenium<sup>[16]</sup>, silver<sup>[17, 18]</sup>, etc.) complexes are used as effective catalysts for various aziridination, cyclopropanation and C–H amination reactions. Very recently, the abundant, low-cost and nontoxic first-row transition metals like manganese<sup>[19, 20]</sup>, iron<sup>[21, 22]</sup>, cobalt<sup>[12, 23, 24]</sup>, nickel<sup>[25]</sup> and copper<sup>[18]</sup> are also found to be excellent

catalysts in diverse nitrene transfer and other nitrogen-containing reactions.

The transition-metal-nitrene complexes mainly involve low-coordinate geometries to avoid the unfavorable antibonding  $d\pi(\text{metal})-p\pi(\text{nitrogen})$  interactions. Thereby, these intermediates commonly exist in three- or four-coordinate trigonal<sup>[26, 28]</sup>, (pseudo)tetrahedral<sup>[29, 30]</sup> and square-planar<sup>[26]</sup> conformations. Lately, a dozen of octahedral coordinate structures were reported with porphyrin derivatives<sup>[31]</sup>, N<sub>4</sub>Py<sup>[32, 33]</sup> and other macrocyclic pentadentate ligands<sup>[34]</sup>. Notably, the electronic structures of cobalt- and iron-nitrenes have attracted much attention. It was found that in the formation of Co(III)-nitrene intermediate, an  $\alpha$  electron transfers from the reductive cobalt center to the nitrene moiety, leaving the unpaired electron residing mainly on the nitrene nitrogen moiety, thus generating the iminyl radical ligand<sup>[12, 18, 19]</sup>. Such transformation was also reported in the intermolecular C–H amination reactions through crucial

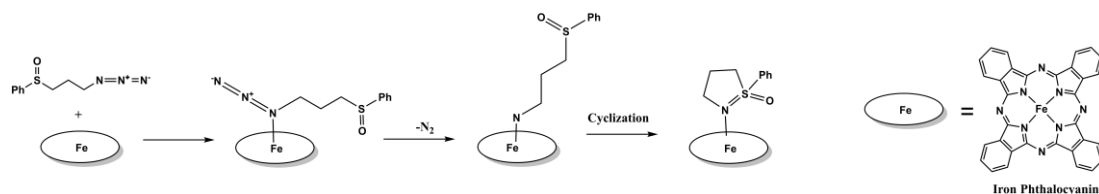
Received 20 July 2020; accepted 12 October 2020

① Supported by the NSFC (21933009) and the Strategic Priority Research Program of the Chinese Academy of Sciences (XDB20000000)

② Corresponding authors. Prof. Li Chun-Sen, E-mail: chunsen.li@fjirsm.ac.cn; Dr. Song Jin-Shuai, E-mail: jssong@zzu.edu.cn

iron-porphyrin-nitrene intermediates by Liu *et al.*<sup>[35]</sup>.

As discussed above, the electronic configuration and reactivity of the iron-nitrene<sup>[35, 36]</sup> have been preliminarily explored in some limited nitrene transfer reactions. Recently, a general method for the synthesis of cyclic sulfoximines by using the commercially available iron phthalocyanine ( $\text{Fe}^{\text{II}}\text{Pc}$ ) was developed by Bolm *et al.*<sup>[37]</sup>. In this reaction,  $\text{Fe}^{\text{II}}\text{Pc}$  was employed to cyclize [(3-azidopropyl)sulfinyl]benzene (**ASB**) to form 4,5-dihydro-3H-isothiazole 1-oxide (**DHI**) through intramolecular sulfoxide imidation reaction (Scheme 1). They



Scheme 1. Iron-catalyzed intramolecular imidations of sulfoxides

## 2 COMPUTATION METHODS

All calculations were performed using the DFT method as implemented in Gaussian 09 program<sup>[38]</sup>. The geometries of all species were optimized in gas phase with the B3LYP<sup>[39, 40]</sup> functional using Ahlrichs def2-SVP basis set<sup>[41, 42]</sup>. Vibrational frequency analysis at the same level of geometry optimization was carried out to check the stationary point or transition state and to obtain the thermodynamic correction to Gibbs free energy. Each transition state has been confirmed by the intrinsic reaction coordinate (IRC) calculations<sup>[43, 44]</sup>. Single-point calculations were performed using the def2-TZVPP basis set<sup>[41, 42]</sup> on the gas-phase optimized geometries considering Grimme's D3 dispersion corrections<sup>[45-47]</sup>. The solvation energy was calculated by polarizable continuum model (PCM)<sup>[48]</sup>, which is a self-consistent reaction field (SCRF) approach, with toluene ( $\epsilon = 2.3741$ ) as solvent. The reported energy was obtained by adding the single-point energy with the free energy correction. ORCA program 4.2<sup>[49]</sup> was also used to calculate the spin natural orbitals.

## 3 RESULTS AND DISCUSSION

### 3.1 DFT optimized iron phthalocyanine nitrene

The calculated results including relative Gibbs free energies, geometric parameters, natural population analysis (NPA) charges, spin densities and Mayer bond orders of the iron phthalocyanine nitrene ( $\text{PcFeNR}$ ,  $\text{R} = (\text{CH}_2)_3(\text{SO})\text{Ph}$ ) in

proposed that this reaction includes two steps: denitration and cyclization, while the vital intermediate was speculated as iron (IV)-nitrene species. To the best of our knowledge, the detailed mechanism of this reaction has not been fully investigated and hence is the focus of the present study. Thus, we seek to elucidate electronic structure, formation mechanism and intramolecular sulfoxide imidation reactivity of the iron (IV)-nitrene species generated from  $\text{Fe}^{\text{II}}\text{Pc}$  and azido-containing sulfoxide substrate.

different spin states are summed up in Table 1, while Fig. 1 presents the geometric and electronic features of  $\text{PcFeNR}$  at the triplet state. The results shown in Table 1 reveal that the triplet state is the ground state followed by the open-shell singlet (IOS), closed-shell singlet (ICS) and quintet states with 2.4, 6.3 and 7.5 kcal/mol higher in energy, respectively. An obvious geometric difference found for quintet species is that the protrusion of iron center from the phthalocyanine plane is the largest with 0.61 Å. The calculated bond length between iron center and the axially ligated nitrogen atom ( $d_{\text{Fe-N}(1)}$ ) for triplet state is 1.71 Å, a distance shorter than the previously reported single bond length of ca 1.9 Å<sup>[35, 50, 51]</sup>, but close to the double bond length of iron nitrene complexes (about 1.70~1.73 Å)<sup>[34, 52]</sup>. Since the triplet state is the lowest energy lying state, the following discussions about  $\text{PcFeNR}$  are mainly focused on this spin state. As shown in Fig. 1, the spin density occupancy numbers on the iron atom and nitrene nitrogen atom are 0.95 and 1.01, respectively, featuring the two-radical centers in triplet  $\text{PcFeNR}$ . NPA charges show that the metal iron atom bears the positive charge while the N(1) atom bears negative charge. These data imply the  $\text{PcFeNR}$  intermediate in triplet state can be described as an iron nitrene anion diradical complex, as suggested by Shaik *et al.*<sup>[53, 54]</sup>. Calculated Mayer bond order for Fe-N(1) at triplet state corresponds to 1.38, suggesting that the bond between iron and N(1) is not a normal double bond. The similar bond order of 1.40 for Fe-N(1) at IOS state is obtained as well, while for ICS state, the bond order corresponds to 1.93, a symbol of normal double bond. This indicates the interaction

between iron and N(1) at triplet and 1OS state is weaker than that in 1CS state, which is consistent with the longer Fe–N(1) bond distance at the same states. For high-energy lying quintet state, the calculated bond order is 1.08, corresponding

to its largest Fe–N(1) bond length of 1.78 Å. Thus, the ground state of PcFeNR complex does not feature a formal iron (IV) configuration in which the bond order of Fe–N(1) should be close to 2.

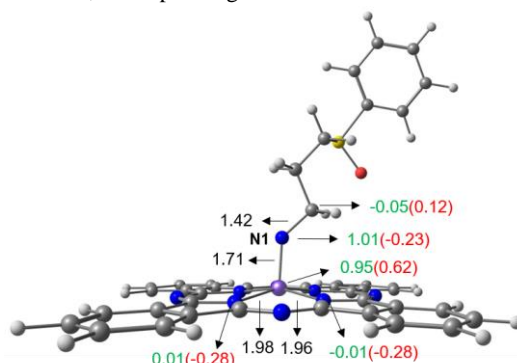


Fig. 1. Highlights of B3LYP/def2-SVP optimized distances (Å, in black), spin densities (green), and NPA charges (red), for the triplet iron phthalocyanine nitrene (PcFeNR)

Table 1. Relative Gibbs Free Energies, Geometric Parameters, NPA Charges, Spin Densities and Mayer Bond Orders of the Iron Phthalocyanine Nitrene at Different Spin States. d is the Protrusion of the Iron Center from the Phthalocyanine Plane. N(1) is the Axially Ligated Nitrogen Atom (see Fig. 1)

	Relative energy (kcal/mol)	Distance (Å)	NPA charge		Spin density		Bond order	d (Å)
		Fe–N(1)	Fe	N(1)	Fe	N(1)	Fe–N(1)	
Triplet	0.0	1.71	0.62	−0.23	0.95	1.01	1.38	0.27
1OS	2.4	1.77	0.64	−0.30	1.10	−0.96	1.40	0.25
1CS	6.3	1.67	0.53	−0.17	–	–	1.93	0.29
Quintet	7.5	1.78	1.15	−0.41	3.96	−0.34	1.08	0.61

A diagram for the molecular orbital interaction of PcFeNR at the triplet state is depicted in Fig. 2. The electronic state configuration is found to be  $(\delta_{xy})^2(\pi_{xz})^1(\pi_{yz})^1(\sigma_z^*)^0(\sigma_x^*)^2(\sigma_y^*)^2$ . The  $\sigma$  bond in the axial Fe–N(1) is mainly generated by the interaction between  $d_z^2(\text{Fe})$  and  $p(\text{N})$  orbitals. Two non-degenerated Fe–N  $\pi$ -antibonding orbitals are formed by strong overlap between the  $d_{xz}$  and  $d_{yz}$  orbitals of iron and  $p_y$  and  $p_x$  orbitals of nitrogen atom. When the  $\sigma$  bond between

Fe and N(1) is formed, the electron-rich iron would transfer  $d$ -electrons to the  $p(\text{N})$  orbitals to form  $\pi$ -back-bonding interaction, which is beneficial to stabilizing the metalloradical complex. Moreover, from Fig. 2, we can find that spin densities are delocalized to the carbon atom adjacent to the proximal nitrogen atom in iron nitrene, thereby further facilitating the metal-to-nitrene donation interaction.

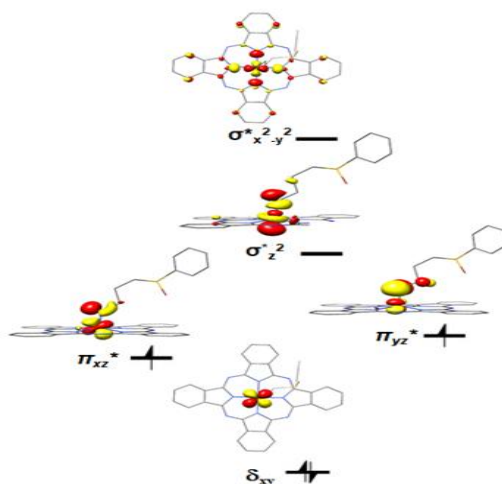


Fig. 2. Schematic of spin natural orbitals for iron phthalocyanine nitrene at triplet state computed by Orca program. Hydrogens are omitted for clarity

It seems that the bonding pattern of PcFeNR at the triplet state is similar to that of iron (IV)-oxo complex, in which two single  $\alpha$ -electrons reside in two nearly degenerated  $\pi^*$  orbitals. However, in PcFeNR complex, the electron-donating nitrogen atom is also bonded to other functional groups. As a consequence, the  $\pi_{xz}^*$  and  $\pi_{yz}^*$  orbitals in PcFeNR complex are no longer degenerated. Besides, the Fe–N bond (1.71 Å) is obviously longer than Fe–O bond (~1.6 Å) in iron (IV)-oxo species, suggesting a higher reactivity for PcFeNR complex. Experimentally, it has been found that the iron-tosylimido complex is much more reactive in sulfoxidation and sulfimination reactions than the homologous iron (IV)-oxo complex<sup>[7]</sup>. Note that the iron-nitrene intermediate may exhibit different reactivities with the various alkyl chain bonding to the proximal electron-donating nitrogen atom, which increases the possibility for functional group design.

### 3.2 Iron phthalocyanine nitrene formation

#### 3.2.1 Energy profiles for denitrification

The proposed catalytic cycle is theoretically investigated using the optimized experimental conditions<sup>[37]</sup>. The calculated results indicate that the entire catalytic cycle contains two reaction steps: denitrification and cyclization.

The free energy profiles for denitrification are shown in Fig. 3. It is seen that for all spin states, the complexation of the separated Fe<sup>II</sup>Pc and **ASB** to reactant cluster (R) is exergonic by more than 8 kcal/mol. And throughout the denitrification, the triplet state is unequivocally the lowest profile. This result is in accord with the calculated spin order of PcFeNR shown above that the triplet state is the ground state. The triplet free energy barrier for denitrification is 23.4 kcal/mol. As will be shown below, the denitrification is the rate-determining step as this calculated free energy barrier is larger than that in the subsequent cyclization step. Recalling that high reaction temperature of 100 °C was needed for the synthesis of cyclic sulfoximines by using Fe<sup>II</sup>Pc<sup>[37]</sup>, the calculated high free energy barrier is in good agreement with experiment. Fig. 4 shows the DFT optimized geometries of the corresponding reactant clusters (R) and transition states (TS<sub>1</sub>). In the R species, three connected nitrogen atoms (N(1)–N(2)–N(3)) in azide group are in linear configuration. However, in TS<sub>1</sub>, a bending structure for N(1)–N(2)–N(3) is obtained. From R to TS<sub>1</sub>, the Fe–N(1) bond length decreases from initial 2.0~2.4 to ~1.8 Å and the N(1)–N(2) bond length increases from 1.23 to 1.63 Å.

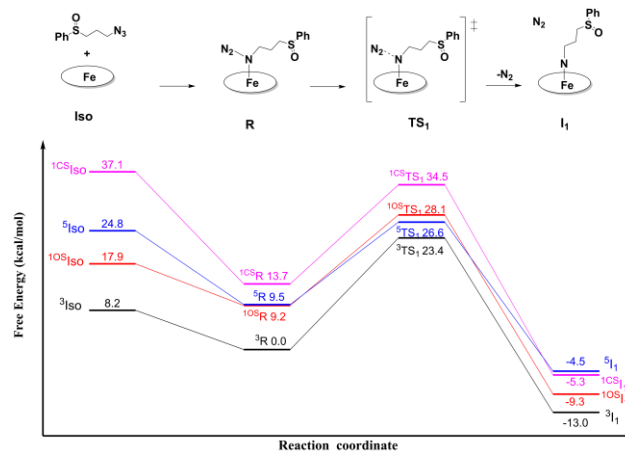


Fig. 3. Free energy profiles for the formation of iron phthalocyanine nitrene species

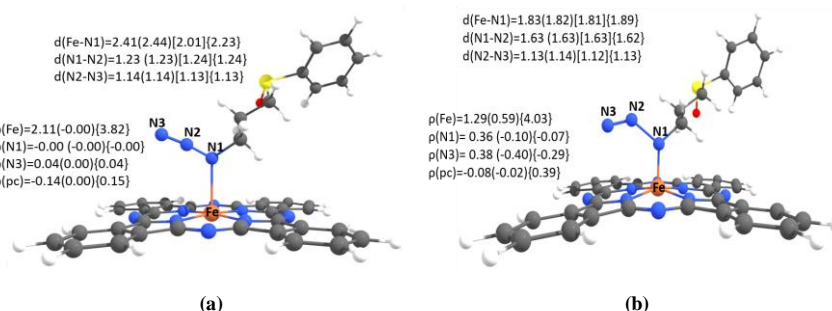


Fig. 4. Optimized structures of R (a) and TS<sub>1</sub> (b) at triplet, 10S (inside the parentheses), 1CS (inside the bracket) and quintet (inside the braces) spin states. The spin densities are represented by  $\rho$ , and distances are given in angstroms

### 3.2.2 Insights into electronic structure change

As shown in Fig. 5, the ground electronic configuration for R species is found to be  $(\delta_{xy})^2(d_{xz})^2(d_{yz})^1(\sigma_z^*)^2(\sigma_{x-y}^*)^0$ , in accord with the spin density on iron (2.10, see Table 2). The process of cleaving N(1)–N(2) bond can be depicted as the consequence of bonding and antibonding interactions between iron and nitrene N(1) atom. Thereby, one  $\alpha$  electron on the  $d_z^2$  orbital of iron (shown in Fig. 5a) transfers to the empty nitrogen-centered  $p_x$  orbital. Furthermore, the singly occupied  $N_{px}$  orbital would interact with the doubly occupied

$d_{xz}$  orbital of iron to form the bonding ( $\pi_{xz}$ ) and antibonding ( $\pi_{xz}^*$ ) molecular orbitals with three electrons in total. Moreover, the one electron occupied  $d_{yz}$  orbital mixed with the doubly occupied  $N_{py}$  orbital also contribute to the similar bonding and antibonding combination. The resultant orbital schematic is shown in Fig. 5b. This result is also consistent with the change of spin densities on iron (2.10 to 1.29) shown in Table 2. We note that such one-electron-transfer is quite a common process in the formation of various metal nitrene/carbene intermediates<sup>[12, 55, 56]</sup>.

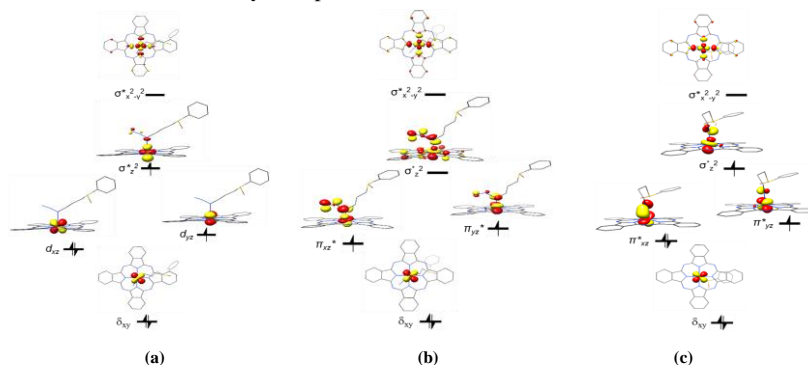


Fig. 5. Schematic of spin natural orbitals for R (a), TS<sub>1</sub> (b) and TS<sub>2</sub> (c) at the triplet state computed in Orca. Hydrogens are omitted for clarity

Table 2. Spin Densities Changes in the Process of Denitrification at Triplet State

	Spin density			
	Fe	N(1)	N(2)	N(3)
R	2.10	0.00	0.00	0.04
TS <sub>1</sub>	1.29	0.36	0.02	0.38
I <sub>1</sub>	0.95	1.00	0.00	0.01

### 3.3 Iron nitrene nucleophilic attack reactivity

Fig. 6 shows the free energy profiles for the cyclization step calculated starting from N<sub>2</sub> eliminated PcFeNR. Again here, the triplet state is the lowest profile throughout the reaction. As such, only results of triplet state are kept in discussions. During the nucleophilic attack of nitrene towards sulfur atom, the Fe–N(1) bond length increases from 1.7 Å in the bent nitrene intermediate to 1.8 Å in the TS<sub>2</sub> and finally to 2.31 Å in the product P, as shown in Table 3. Simultaneously, one electron transfers from nitrene moiety back to the iron center as the spin density on iron accordingly increases to 2.27 in <sup>3</sup>TS<sub>2</sub> vs 0.96 in <sup>3</sup>I<sub>3</sub>. The free energy barrier for this

intramolecular imidation is calculated to be 9.6 kcal/mol at the triplet state. As such, the denitrification process shown above is found to be the rate-determining step as it needs to overcome higher free energy barrier. This result is consistent with previously reported nitrene transfer reactions catalyzed by iron porphyrins and other metal catalysts<sup>[56, 57, 58]</sup>. The formation of intramolecular imidation product <sup>3</sup>P is exergonic by more than 48 kcal/mol albeit to release the free **DHI** is less exergonic. Thus, the whole process for converting azide-containing sulfoxide to cyclic sulfoximine catalyzed by PcFeNR is highly thermodynamically favorable.

Table 3. Geometric Parameters and Spin Density Changes in the Process of Nucleophilic Reaction at Triplet State

	Distance (Å)		Spin density			
	Fe–N(1)	N(1)–S	Fe	N(1)	S	O
I <sub>2</sub>	1.71	4.65	0.95	1.01	0.00	0.00
I <sub>3</sub>	1.71	2.99	0.96	0.99	0.00	0.00
TS <sub>2</sub>	1.90	2.20	2.27	0.01	−0.10	−0.09
P	2.31	1.57	2.12	0.03	0.01	0.00

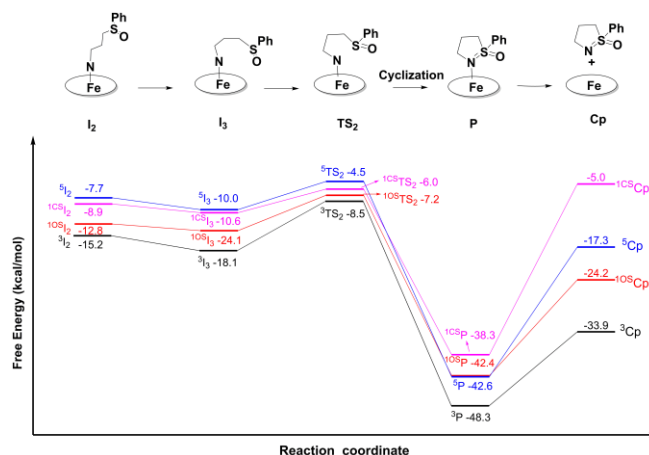


Fig. 6. Free energy profiles for the formation of sulfoximine through nucleophilic attack

In the cyclization step, an  $\alpha$  electron transfers from the nitrogen-centered orbitals back to iron center  $d_z^2$  orbital. At the same time, both  $\sigma_{N-S}$  and  $\pi_{N-S}$  orbitals are formed in the  $^3TS_2$  when the nitrene nitrogen approaches sulfur atom and further interacts with each other. The electronic configuration of  $^3TS_2$  for  $d$ -block is  $(\delta_{xy})^2(\pi_{xz}^*)^2(\pi_{yz}^*)^1(\sigma_z^*)^1(\sigma_x^*)^2(\sigma_y^*)^2$  (see Fig. 5b), in agreement with the spin density 2.27 on iron, indicating the iron nitrene radical is reduced to ferrous complex at this stage.

In order to investigate the influencing factors of the reaction energy barrier caused by azido sulfoxide substrate, we have performed corresponding calculations for the reactions with substrates containing different substituents ( $-N=N^+=N-R$ ,  $R=(CH_2)(CH_3)_2(CH_2)(SO)Ph$ ,  $(CH_2)_2(CH)(CH_3)(SO)Ph$  and  $(CH_2)_3(SO)C_6H_5$ , respectively) which have been employed in experiment<sup>[37]</sup>. We only explored the denitration process at triplet spin state as it has been found above that the denitration is the rate-determining step. As shown in Fig. 7, substrates with

methyl-substituted zaidoalkyl chains (**Sub-2** and **Sub-3**) require slightly higher barriers (24.8 and 25.2 kcal/mol, respectively) than **Sub-1** (23.4 kcal/mol). This is in good agreement with the experiment that higher reaction temperature (140 °C) and more dosage catalysts are required to promote the imidation reactions using **Sub-2** and **Sub-3** as substrates<sup>[37]</sup>. In addition, with the non-aromatic substrate **Sub-4**, the reaction barrier calculated is 24.7 kcal/mol, again a slightly higher barrier than **Sub-1**, which is corresponding to the lower yield when using **Sub-4** in the experiment<sup>[37]</sup>. Thus, the substrates with electron-donating groups and aliphatic substituents are energy unfavorable for the denitration step so that they exhibit low reactivity and need more harsh experimental conditions. In other words, our results suggest that azido sulfoxide substrates with electron-withdrawing substituents may be energy favorable for the dinitrogen reaction and thus promote the cyclic sulfoximines catalyzed by  $Fe^{II}Pc$ .

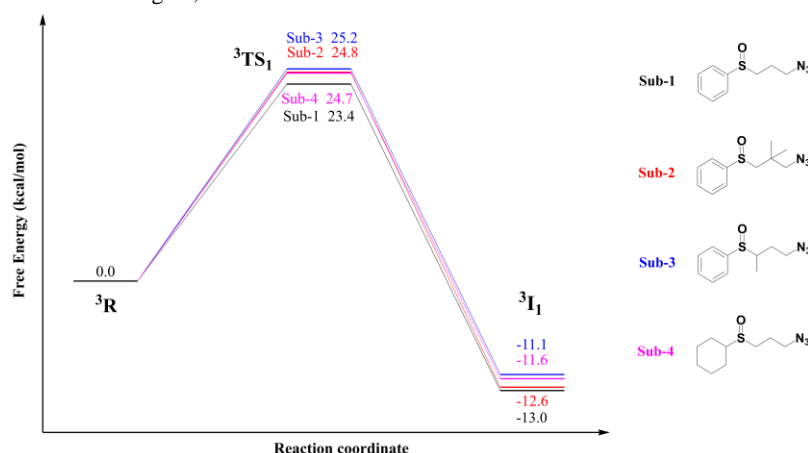


Fig. 7. Free energy profiles of denitration for different substituents at triplet state

## 4 CONCLUSION

Our DFT calculations show that intramolecular imidation reaction for the synthesis of cyclic sulfoximine by using iron phthalocyanine as catalyst and azido sulfoxide as substrate contains two steps. First, azido-containing sulfoxide substrate releases dinitrogen to yield iron nitrene radical intermediate, which is found with higher energy barrier and thus is the rate-limiting step in the whole process. Second, the resulting iron nitrene intermediate [FePcN(CH<sub>2</sub>)<sub>3</sub>(SO)Ph] undergoes a low-barrier intramolecular imidation to accomplish the

cyclization of sulfoxide. The ground state for the [FePcN(CH<sub>2</sub>)<sub>3</sub>(SO)Ph] intermediate is triplet spin state with two unpaired electrons residing on the iron and nitrene moiety, respectively. Theoretical analysis on four substrates with different substituents show that the electron donating groups play an adverse role in the formation of iron nitrene intermediates. This work may provide deeper insight for understanding the electronic property of iron-based nitrene intermediates and developing better substrates for the synthesis of heterocyclic sulfoximine.

## REFERENCE

- (1) Roughley, S. D.; Jordan, A. M. The medicinal chemist's toolbox: an analysis of reactions used in the pursuit of drug candidates. *J. Med. Chem.* **2011**, 54, 3451–3479.
- (2) Mehn, M. P.; Peters, J. C. Mid-to high-valent imido and nitrido complexes of iron. *J. Inorg. Biochem.* **2006**, 100, 634–643.
- (3) Holland, P. L. Electronic structure and reactivity of three-coordinate iron complexes. *Acc. Chem. Res.* **2008**, 41, 905–914.
- (4) Manchillo, O. G.; Dallimore, J.; Plant, A.; Bolm, C. Iron(II) triflate as an efficient catalyst for the imination of sulfoxides. *Org. Lett.* **2009**, 11, 2429–2432.
- (5) Manchillo, O. G.; Dallimore, J.; Plant, A.; Bolm, C. Synthesis of sulfoximines and sulfilimines with aryl and pyrazolylmethyl substituents. *Adv. Synth. Catal.* **2010**, 352, 309–316.
- (6) Wang, J.; Frings, M.; Bolm, C. Enantioselective nitrene transfer to sulfides catalyzed by a chiral iron complex. *Angew. Chem. Int. Ed.* **2013**, 52, 8661–8665.
- (7) Kumar, S.; Faponle, A. S.; Barman, P.; Vardhaman, A. K.; Sastri, C. V.; Kumar, D.; Visser, S. P. D. Long-range electron transfer triggers mechanistic differences between iron(IV)-oxo and iron(IV)-imido oxidants. *J. Am. Chem. Soc.* **2014**, 136, 17102–17115.
- (8) Manchillo, O. G.; Bolm, C. Iron-catalyzed imination of sulfoxides and sulfides. *Org. Lett.* **2006**, 8, 2349–2352.
- (9) Barman, D. N.; Liu, P.; Houk, K. N.; Nicholas, K. M. On the mechanism of ligand-assisted, copper, catalyzed benzylic amination by chloramine-T. *Organometallics* **2010**, 29, 3404–3412.
- (10) Vyas, R.; Gao, G. Y.; Harden, J. D.; Zhang, X. P. Iron(III) porphyrin catalyzed aziridination of alkenes with bromamine-T as nitrene source. *Org. Lett.* **2004**, 6, 1907–1910.
- (11) Lebel, H.; Huard, K.; Lectard, S. N-tosyloxycarbamates as a source of metal nitrenes: rhodium-catalyzed C-H insertion and aziridination reactions. *J. Am. Chem. Soc.* **2005**, 127, 14198–14199.
- (12) Suarez, A. I. O.; Jiang, H. L.; Zhang, X. P.; De Bruin, B. The radical mechanism of cobalt(II) porphyrin-catalyzed olefin aziridination and the importance of cooperative H-bonding. *Dalton Trans.* **2011**, 40, 5697–5705.
- (13) Intrieri, D.; Zardi, P.; Caselli, A.; Gallo, E. Organic azides: "energetic reagents" for the intermolecular amination of C–H bonds. *Chem. Commun.* **2014**, 50, 11440–11453.
- (14) Geer, A. M.; Tejel, C.; Lopez, J. A.; Ciriano, M. A. Terminal imido rhodium complexes. *Angew. Chem. Int. Ed.* **2014**, 53, 5614–5618.
- (15) Scheibel, M. G.; Wu, Y. L.; Stuckl, A. C.; Krause, L.; Carl, E.; Stalke, D.; De Bruin, B.; Schneider, S. Synthesis and reactivity of a transient, terminal nitrido complex of rhodium. *J. Am. Chem. Soc.* **2013**, 135, 17719–17722.
- (16) Manca, G.; Gallo, E.; Intrieri, D.; Mealli, C. DFT mechanistic proposal of the ruthenium porphyrin-catalyzed allylic amination by organic azides. *ACS Catal.* **2014**, 4, 823–832.
- (17) Zhang, J.; Shan, C. H.; Zhang, T.; Song, J. S.; Liu, T.; Lan, Y. Computational advances aiding mechanistic understanding of silver-catalyzed carbene/nitrene/silylene transfer reactions. *Coord. Chem. Rev.* **2019**, 382, 69–84.
- (18) Díaz-Requejo, M. M.; Pérez, P. J. The Tp<sup>x</sup>M core in Csp<sup>3</sup>–H bond functionalization reactions: comparing carbene, nitrene, and oxo insertion processes (Tp<sup>x</sup> = scorpionate ligand; M = Cu, Ag). *Eur. J. Inorg. Chem.* **2020**, 879–885.
- (19) Wang, J. P.; Zheng, K. C.; Li, T.; Zhan, X. J. Mechanism and chemoselectivity of mn-catalyzed intramolecular nitrene transfer reaction: C–H

- amination vs. C=C aziridination. *Catalysts* **2020**, 10, 292–303.
- (20) Ning, T. R.; Song, J. S.; Wei, J.; Zhang, M. Y.; Lu, Q. Q.; Huang, J.; Li C. S. Control of the electronic structure of manganese nitrido complexes by pararing substituents: a theoretical study. *Chin. J. Struct. Chem.* **2018**, 37, 1541–1549.
- (21) Che, C. M.; Lo, V. K. Y.; Zhou, C. Y.; Huang, J. S. Selective functionalisation of saturated C–H bonds with metalloporphyrin catalysts. *Chem. Soc. Rev.* **2011**, 40, 1950–1975.
- (22) Zheng, J.; Liu, Z. Y.; Jin, X. J.; Dang, Y. F. Unveiling the mechanism and regioselectivity of iron-dipyrinato-catalyzed intramolecular C(sp<sup>3</sup>)-H amination of alkyl azides. *Catal. Sci. Technol.* **2019**, 9, 1279–1288.
- (23) Hopmann, K. H.; Ghosh, A. Mechanism of cobalt-porphyrin-catalyzed aziridination. *ACS Catal.* **2011**, 1, 597–600.
- (24) Lyaskovskyy, V.; Suarez, A. I. O.; Lu, H. J.; Jiang, H. L.; Zhang, X. P.; De Bruin, B. Mechanism of cobalt(II) porphyrin-catalyzed C–H amination with organic azides: radical nature and H-atom abstraction ability of the key cobalt(III)-nitrene intermediates. *J. Am. Chem. Soc.* **2011**, 133, 12264–12273.
- (25) Camasso, N. M.; Canty, A. J.; Ariafard, A.; Sanford, M. S. Experimental and computational studies of high-valent nickel and palladium complexes. *Organometallics* **2017**, 36, 4382–4393.
- (26) Baek, Y.; Betley, T. A. Catalytic C–H amination mediated by dipyrin cobalt imidos. *J. Am. Chem. Soc.* **2019**, 141, 7797–7806.
- (27) Wang, L.; Hu, L. R.; Zhang, H. Z.; Chen, H.; Deng, L. Three-coordinate iron(IV) bisimido complexes with aminocarbene ligation: synthesis, structure, and reactivity. *J. Am. Chem. Soc.* **2015**, 137, 14196–14207.
- (28) Reckziegel, A.; Pietzonka, C.; Kraus, F.; Werncke, C. G. C–H bond activation by an imido cobalt(III) and the resulting amido cobalt(II) complex. *Angew. Chem. Int. Ed.* **2020**, 59, 8527–8531.
- (29) Searles, K.; Fortier, S.; Khusniyarov, M. M.; Carroll, P. J.; Sutter, J.; Meyer, K. A *cis*-divacant octahedral and mononuclear iron(IV) imide. *Angew. Chem. Int. Ed.* **2014**, 53, 14139–14143.
- (30) Liu, Y.; Du, J. Z.; Deng, L. Synthesis, structure, and reactivity of low-spin cobalt(II) imido complexes [(Me<sub>3</sub>P)<sub>3</sub>Co(NAr)]. *Inorg. Chem.* **2017**, 56, 8278–8286.
- (31) Fantauzzi, S.; Caselli, A.; Gallo, E. Nitrene transfer reactions mediated by metallo-porphyrin complexes. *Dalton Trans.* **2009**, 5434–5443.
- (32) Vardhaman, A. K.; Lee, Y. M.; Jung, J.; Ohkubo, K.; Nam, W.; Fukuzumi, S. Enhanced electron transfer reactivity of a nonheme iron(IV)-imido complex as compared to the iron(IV)-oxo analogue. *Angew. Chem. Int. Ed.* **2016**, 55, 3709–3713.
- (33) Vardhaman, A. K.; Barman, P.; Kumar, S.; Sastri, C. V.; Kumar, D.; De Visser, S. P. Comparison of the reactivity of nonheme iron(IV)-oxo versus iron(IV)-imido complexes: which is the better oxidant? *Angew. Chem. Int. Ed.* **2013**, 52, 12288–12292.
- (34) Sabenya, G.; Gamba, I.; Gomez, L.; Clemancey, M.; Frisch, J. R.; Klinker, E. J. Octahedral iron(IV)-tosylimido complexes exhibiting single electron-oxidation reactivity. *Chem. Sci.* **2019**, 10, 9513–9529.
- (35) Li, X. Y.; Dong, L. H.; Liu, Y. Theoretical study of iron porphyrin nitrene: formation mechanism, electronic nature, and intermolecular C–H amination. *Inorg. Chem.* **2020**, 59, 1622–1632.
- (36) Conradie, J.; Ghosh, A. Electronic structure of an iron-porphyrin-nitrene complex. *Inorg. Chem.* **2010**, 49, 243–248.
- (37) Yu, H.; Li, Z.; Bolm, C. Three-dimensional heterocycles by iron-catalyzed ring-closing sulfoxide imidation. *Angew. Chem. Int. Ed.* **2018**, 57, 12053–12056.
- (38) Frisch, M. J.; Trucks, G. W.; Schlegel, H. B.; Scuseria, G. E.; Robb, M. A.; Cheeseman, J. R.; Scalmani, G.; Barone, V.; Mennucci, B.; Petersson, G. A.; Nakatsuji, H.; Caricato, M.; Li, X.; Hratchian, H. P.; Izmaylov, A. F.; Bloino, J.; Zheng, G.; Sonnenberg, J. L.; Hada, M.; Ehara, M.; Toyota, K.; Fukuda, R.; Hasegawa, J.; Ishida, M.; Nakajima, T.; Honda, Y.; Kitao, O.; Nakai, H.; Vreven, T.; Montgomery, J. A. Jr.; Peralta, J. E.; Ogliaro, F.; Bearpark, M.; Heyd, J. J.; Brothers, E.; Kudin, K. N.; Staroverov, V. N.; Keith, T.; Kobayashi, R.; Normand, J.; Raghavachari, K.; Rendell, A.; Burant, J. C.; Iyengar, S. S.; Tomasi, J.; Cossi, M.; Rega, N.; Millam, J. M.; Klene, M.; Knox, J. E.; Cross, J. B.; Bakken, V.; Adamo, C.; Jaramillo, J.; Gomperts, R.; Stratmann, R. E.; Yazyev, O.; Austin, A. J.; Cammi, R.; Pomelli, C.; Ochterski, J. W.; Martin, R. L.; Morokuma, K.; Zakrzewski, V. G.; Voth, G. A.; Salvador, P.; Dannenberg, J. J.; Dapprich, S.; Daniels, A. D.; Farkas, O.; Foresman, J. B.; Ortiz, J. V.; Cioslowski, J.; Fox, D. J. *Gaussian 09, Revision D. 01*; Gaussian, Inc.: Wallingford CT **2013**.
- (39) Becke, A. D. Density-functional thermochemistry. III. The role of exact exchange. *J. Chem. Phys.* **1993**, 98, 5648–5652.
- (40) Miehlich, B.; Savin, A.; Stoll, H.; Preuss, H. Results obtained with the correlation energy density functionals of Becke and Lee, Yang and Parr. *Chem. Phys. Lett.* **1989**, 157, 200–206.
- (41) Weigend, F.; Ahlrichs, R. Balanced basis sets of split valence, triple zeta valence and quadruple zeta valence quality for H to Rn: design and



- assessment of accuracy. *Phys. Chem. Chem. Phys.* **2005**, 7, 3297–3305.
- (42) Zheng, J.; Xu, X.; Truhlar, D. G. Minimally augmented Karlsruhe basis sets. *Theor. Chem. Acc.* **2011**, 128, 295–305.
- (43) Fukui, K. A formulation of the reaction coordinate. *J. Phys. Chem.* **1970**, 74, 4161–4163.
- (44) Fukui, K. The path of chemical reactions - the IRC approach. *Acc. Chem. Res.* **1981**, 14, 363–368.
- (45) Grimme, S. Semiempirical GGA-type density functional constructed with a long-range dispersion correction. *J. Comput. Chem.* **2006**, 27, 1787–1799.
- (46) Grimme, S.; Antony, J.; Ehrlich, S.; Krieg, H. A consistent and accurate *ab initio* parametrization of density functional dispersion correction (DFT-D) for the 94 elements H–Pu. *J. Chem. Phys.* **2010**, 132, 154104–19.
- (47) Grimme, S.; Ehrlich, S.; Goerigk, L. Effect of the damping function in dispersion corrected density functional theory. *J. Comput. Chem.* **2011**, 32, 1456–1465.
- (48) Miertu, S.; Scrocco, E.; Tomasi, J. Electrostatic interaction of a solute with a continuum. A direct utilization of *ab initio* molecular potentials for the prevision of solvent effects. *Chem. Phys.* **1981**, 55, 117–129.
- (49) Neese, F.; Wennmohs, F.; Becker, U.; Riplinger, C. The ORCA quantum chemistry program package. *J. Chem. Phys.* **2020**, 152, 224108–18.
- (50) Conradie, J.; Ghosh, A. Electronic structure of an iron-porphyrin-nitrene complex. *Inorg. Chem.* **2010**, 49, 243–248.
- (51) Wang, J.; Gao, H.; Yang, L.; Gao, Y. Q. Role of engineered iron-haem enzyme in reactivity and stereoselectivity of intermolecular benzylic C–H bond amination. *ACS Catal.* **2020**, 10, 5318–5327.
- (52) Spasyuk, D. M.; Carpenter, S. H.; Kefalidis, C. E.; Piers, W. E.; Neidig, M. L.; Maron, L. Facile hydrogen atom transfer to iron(III) imido radical complexes supported by a dianionic pentadentate ligand. *Chem. Sci.* **2016**, 7, 5939–5944.
- (53) Sharon, D. A.; Mallick, D.; Wang, B.; Shaik, S. Computation sheds insight into iron porphyrin carbenes' electronic structure, formation, and N–H insertion reactivity. *J. Am. Chem. Soc.* **2016**, 138, 9597–9610.
- (54) Khade, R. L.; Zhang, Y. Catalytic and biocatalytic iron porphyrin carbene formation: effects of binding mode, carbene substituent, porphyrin substituent, and protein axial ligand. *J. Am. Chem. Soc.* **2015**, 137, 7560–7563.
- (55) Hopmann, K. H.; Ghosh, A. Mechanism of cobalt-porphyrin-catalyzed aziridination. *ACS Catal.* **2011**, 1, 597–600.
- (56) Lyaskovskyy, V.; Suarez, A. I. O.; Lu, H.; Jiang, H.; Zhang, X. P.; De Bruin, B. Mechanism of cobalt(II) porphyrin-catalyzed C–H amination with organic azides: radical nature and H-atom abstraction ability of the key cobalt(III)-nitrene intermediates. *J. Am. Chem. Soc.* **2011**, 133, 12264–12273.
- (57) Ansari, A. J.; Pathare, R. S.; Maurya, A. K.; Agnihotri, V. K.; Khan, S.; Roy, T. K. Synthesis of diverse nitrogen heterocycles via palladium-catalyzed tandem azide-isocyanide cross-coupling/cyclization: mechanistic insight using experimental and theoretical studies. *Adv. Synth. Catal.* **2018**, 360, 290–297.
- (58) Xiao, X. S.; Hou, C.; Zhang, Z. H.; Ke, Z. F.; Lan, J. Y.; Jiang, H. F. Iridium(III)-catalyzed regioselective intermolecular unactivated secondary C<sub>sp</sub><sup>3</sup>–H bond amidation. *Angew. Chem. Int. Ed.* **2016**, 55, 11897–11901.